RSC Advances

PAPER

View Article Online
View Journal | View Issue

Cite this: *RSC Adv.*, 2020, **10**, 11499

Phase junction enhanced photocatalytic activity of Ga_2O_3 nanorod arrays on flexible glass fiber fabric†

Hanlin Sun,[a] Liying Zhang,[a] Jingyan Yu,[a] Shunli Wang,*[a] Daoyou Guo,[a] Chaorong Li,[a] Fengmin Wu,[a] Aiping Liu,[a] Peigang Li[b] and Weihua Tang[b]

Received 15th February 2020
Accepted 10th March 2020

DOI: 10.1039/d0ra01461c

rsc.li/rsc-advances

Ga_2O_3 nanostructures hold great potential applications in photocatalytic fields due to their stability, high efficiency and environmental friendliness. The construction of phase junction has been proved to be one of the most effective strategies for enhancing Ga_2O_3 photocatalytic activity. However, the influence of the formation process at the interface of the phase junction on the photocatalytic activity of Ga_2O_3 nanostructures is far less well understood. In this work, for the first time, large-area Ga_2O_3 nanorod arrays (NRAs) with controllable α/β phase junction were prepared *in situ* on a flexible glass fiber fabric by a facile and environmentally friendly three-step method. The α/β-Ga_2O_3 phase junction NRAs exhibit an ultra-high photocatalytic degradation rate of 97% during Ultraviolet (UV) irradiation for 60 min, which is attributed to a unique phase junction promoting efficient charge separation. However, the photocatalytic activity of α/β-Ga_2O_3 phase junction NRAs is not evident in the early phase transition, possibly due to the presence of defects acting as charge recombination centers.

1. Introduction

With the continuous development of the social economy, environmental pollution has become an increasingly serious problem, prompting humans to continuously explore new solutions.[1–6] Photocatalytic reaction, as a simple, efficient and cost-effective method, has promising applications in the removal of environmental pollutants and attracted wide attention.[7–13] Recently, various metal oxides with d^{10} (In^{3+}, Ga^{3+}, Ge^{4+}, Sn^{4+}) configurations have been reported as effective photocatalysts for photodegradation of various organic pollutants.[14,15] Ga_2O_3 is a typical representative among them.[16]

With a wide bandgap (4.2–4.9 eV) and excellent physical and chemical properties, Ga_2O_3 is recognized as one of the most promising semiconductors of this century.[17–22] It has extensively been applied to power devices,[23–25] solar-blind ultraviolet (UV) photodetectors,[26–29] gas sensors,[30] solar cells[31] and photocatalysis.[32,33] For photocatalysis applications, related studies claim that Ga_2O_3 can theoretically exhibit better and more stable photocatalytic activity than commercial TiO_2 and realize the degradation of refractory pollutants.[34,35] This is attributed to the extraordinary redox capability of photogenerated electron–hole pairs.[1,36,37] Furthermore, Ga_2O_3 is also widely accepted as an environmentally friendly material with low cost and high chemical stability.[38] Many methods have been investigated to further improve the photocatalytic activity of Ga_2O_3, including morphology controlling, doping, surface modification and semiconductor coupling.[39–44] Nitu Syed *et al.* reported a two-step method for the synthesis of porous α-Ga_2O_3 nanosheets from liquid metal gallium, explaining that the excellent photocatalytic activity of α-Ga_2O_3 originated from the narrowed bandgap caused by trap states.[1] Han *et al.* revealed that the modification of *in situ* Ag nanoparticles can effectively improve the photocatalytic property of Ga_2O_3 for hydrogen evolution.[39] Zhang *et al.* incorporated solvothermally synthesized Ga_2O_3 nanoparticles into liquid metal/metal oxide frameworks to form enhanced photocatalytic systems.[41] Xu *et al.* fabricated two-dimensional TiO_2–Ga_2O_3 p–n heterostructures, demonstrating the contribution of heterostructures in enhancing photocatalytic activity.[45]

Furthermore, the construction of appropriate phase junction structure in Ga_2O_3 can also significantly enhance photocatalytic activity.[46–48] Liu *et al.* demonstrated that the mesopores and heterojunction in the mixed-phase Ga_2O_3 are responsible for enhancing photocatalytic activity.[7] However, the influence of the formation process at the interface of the phase junction on the photocatalytic activity of Ga_2O_3 nanostructures has not been fully understood. For example, phase transformation is a process from the surface to the bulk, and different thicknesses of phase interface may result in various photocatalytic activities.[49] Therefore, an in-depth understanding of junction-related issues will aid in the design and preparation of efficient Ga_2O_3

[a]*Key Laboratory of Optical Field Manipulation of Zhejiang Province, Center for Optoelectronics Materials and Devices, Department of Physics, Zhejiang Sci-Tech University Hangzhou, 310018, China. E-mail: slwang@zstu.edu.cn*

[b]*State Key Laboratory of Information Photonics and Optical Communications, Information Functional Materials and Devices, School of Science, Beijing University of Posts and Telecommunications, Beijing 100876, China*

† Electronic supplementary information (ESI) available. See DOI: 10.1039/d0ra01461c

nanostructured photocatalysts. On the other hand, almost all of the reported Ga_2O_3 nanostructured photocatalysts are currently applied in suspension systems. The disadvantages of photocatalysts, such as agglomeration, inadequate illumination and difficulty in recovery, restrict their large-scale practical applications. Glass fiber fabric as a support for *in situ* growth of Ga_2O_3 nanostructures is expected to effectively overcome this difficulty.[18] To the best of our knowledge, there are no reports of *in situ* preparation of Ga_2O_3 nanostructures on glass fiber fabric for the application of photocatalytic degradation.

Herein, for the first time, we reported a facile and environmentally friendly three-step method for *in situ* preparation of large-area Ga_2O_3 nanorod arrays (NRAs) with controllable α/β phase junction on a flexible glass fiber fabric. The as-prepared α/β-Ga_2O_3 phase junction NRAs exhibited excellent photocatalytic activity for the degradation of Rhodamine B (RhB) aqueous solution. In addition, the mechanism of photocatalytic activity enhancement was discussed and compared with related literature.

2. Experimental

2.1. Materials

Glass fiber fabric, model TS-BXB, specification 0.06 MM × 1.20 M, obtained from Hangzhou Gaojing Fine Chemical Industry Co., Ltd. The glass fiber fabrics were cut into a size of approximately 20 × 20 mm^2 as the substrate of Ga_2O_3 NRAs. Rhodamine B (RhB), gallium nitrate hydrate ($Ga(NO_3)_3 \cdot nH_2O$) were purchased from Shanghai Saen Chemical Technology Co., Ltd. Fluorine doped tin oxide (FTO) conductive glass (14 Ω cm^{-2}, size: 10 × 20 × 2.2 mm^3) was made by Japan Nippon Sheet Glass Co., Ltd. Sodium sulphate (Na_2SO_4) was got from Tianjin Yongda Chemical Regent Co., Ltd. All chemicals are analytical grade.

2.2. Sample preparation

The preparation of Ga_2O_3 NRAs involves the following three steps. In the first step, a SnO_2 thin film was fabricated by radio frequency magnetron sputtering on the surface of the cleaned glass fiber fabric, which was used as a growth seed layer of Ga_2O_3. The growth temperature and Ar gas pressure were fixed at 550 °C and 0.8 Pa, respectively. The second step is to prepare GaOOH nanorod precursor by hydrothermal method. Here, 0.20 g of $Ga(NO_3)_3 \cdot nH_2O$ was dissolved in 30 mL of DI water to prepare a growth solution. Then the substrates glass fiber fabric completed in the first step was placed in the growth solution and transferred separately into a 50 mL Teflon-lined stainless steel autoclave for hydrothermal treatment at 150 °C for 12 h. After the solution was naturally cooled down to room temperature, the precipitates were filtered and washed with DI water, then dried in air at 80 °C for 2 h to obtain GaOOH NRAs precursors. The last step, the as-prepared precursors were annealed at 400 °C for 4 h in air to obtain α-Ga_2O_3 NRAs. The detailed synthesis is schematically demonstrated in Fig. 1. Further, other samples were obtained by annealing α-Ga_2O_3 NRAs in air at 700 °C for different times from 20 min to 120 min.

2.3. Characterization

The crystal structure of samples was analyzed by a Bruker D8 DISCOVER X-ray diffractometer (XRD). UV-Raman spectra were recorded on a Jobin-Yvon T64000 triple-stage spectrograph with spectral resolution of 2 cm^{-1}. The thermal behavior of the GaOOH nanorod was investigated by thermal gravimetric analyzer (Pyris1 TGA). For the morphological and microstructural analysis, a Hitachi S-4800 field-emission scanning electron microscope (SEM) equipped and a JEOL JEM-2100 transmission electron microscopy (TEM) were utilized. The ultraviolet-visible (UV-vis) absorption spectra were taken using a Hitachi U-3900 UV-vis spectrophotometer. The chemical composition of samples was characterized by a Thermo Scientific K-Alpha X-ray photoelectron spectroscopy (XPS).

2.4. Photocatalytic experiments

In this experiment, the glass fiber fabric with Ga_2O_3 NRAs were dropped into 50 mL of RhB aqueous solution (2×10^{-5} M) and

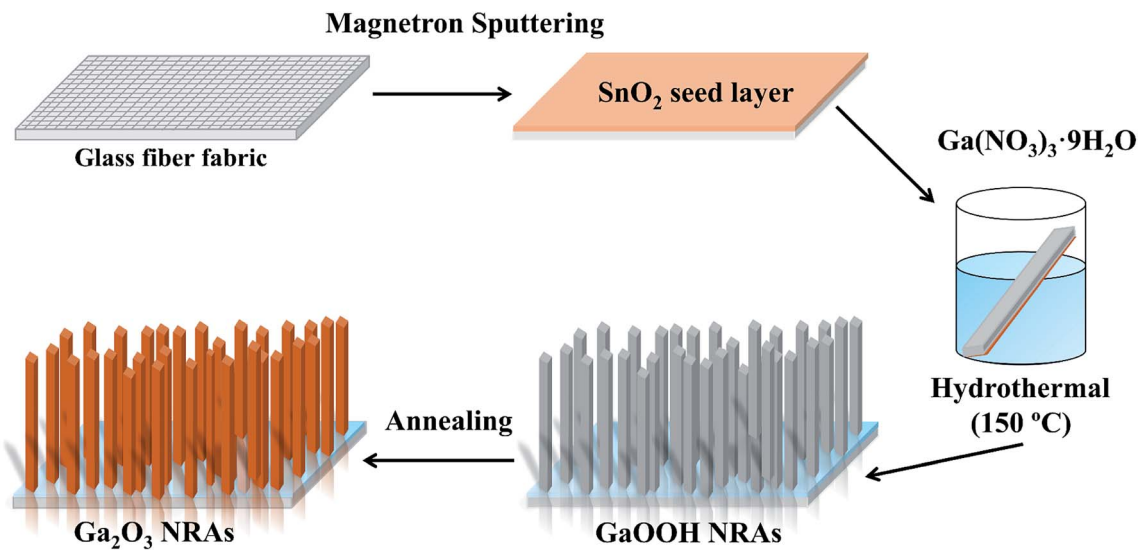

Fig. 1 Schematic illustration of the preparation process of α-Ga_2O_3 NRAs.

placed in the dark for 30 min to ensure adsorption–desorption equilibrium was reached. Then irradiated reaction solution with a 10 W UV light lamp ($\lambda = 254$ nm). The light intensity of the UV lamp was always maintained at 1.0 mW cm^{-2}. During the process, about 3 mL of solution was withdrawn from the reaction system at a given time interval (10 min) for absorbance testing by UV-vis spectrophotometry.

2.5. Mott–Schottky measurement

For Mott–Schottky measurements, 5 mg Ga_2O_3 NRAs powder was scraped from the glass fiber fabric and dispersed in 2 mL of absolute ethanol, followed by the addition of 20 μL of 0.5% Nafion. After the mixed solution was sonicated for 1 h, 0.5 mL was transferred onto a FTO conductive glass. The resulting electrodes were dried in air and further heated at 150 °C for 1 h under a N_2 gas flow. The electrochemical measurements were performed in a three-electrode configuration system using a CHI 760E electrochemical workstation (CH Instruments, China), including the as-prepared FTO working electrodes (with an active area of 1.0 cm^2), Pt foil as the counter electrode and saturated calomel electrode (SCE) as the reference electrode. 0.5 M Na_2SO_4 aqueous solution was used as the electrolyte.

3. Results and discussion

Fig. 2(a) shows the XRD patterns of as-synthesized GaOOH and α-Ga_2O_3 NRAs. All the peaks can be indexed to the orthorhombic GaOOH phase (JCPDS no. 06-0180) except the diffraction peak of the SnO_2 seed layer. After annealing GaOOH at 400 °C for 4 h, the observed diffraction peaks occur at new locations, indicating that the GaOOH is completely converted into α-Ga_2O_3 of the corundum structure (JCPDS no. 06-0503).[50] The phase transition of α-Ga_2O_3 at 700 °C for various times was also analyzed by XRD, and the corresponding results are shown in Fig. 2(b). With α-Ga_2O_3 annealed at 700 °C for 30 min, a diffraction peak corresponding to the (111) plane attributed to monoclinic β-Ga_2O_3 is detected, and it becomes stronger with the further increase of annealing time. Ga_2O_3 with different phase structures can be obtained during annealing for 30–90 min. No diffraction peak assigned to α-Ga_2O_3 is observed through annealing for 120 min, suggesting that the α-Ga_2O_3 is totally transformed into β-Ga_2O_3 at this point.

UV Raman spectroscopy was also used to monitor the α to β phase transformation of Ga_2O_3. As shown in Fig. 2(c), it is worth noting that the typical characteristic Raman bands of β-Ga_2O_3 at 198 cm^{-1} and 414 cm^{-1} can be clearly observed after annealing α-Ga_2O_3 at 700 °C for 20 min, in addition to the

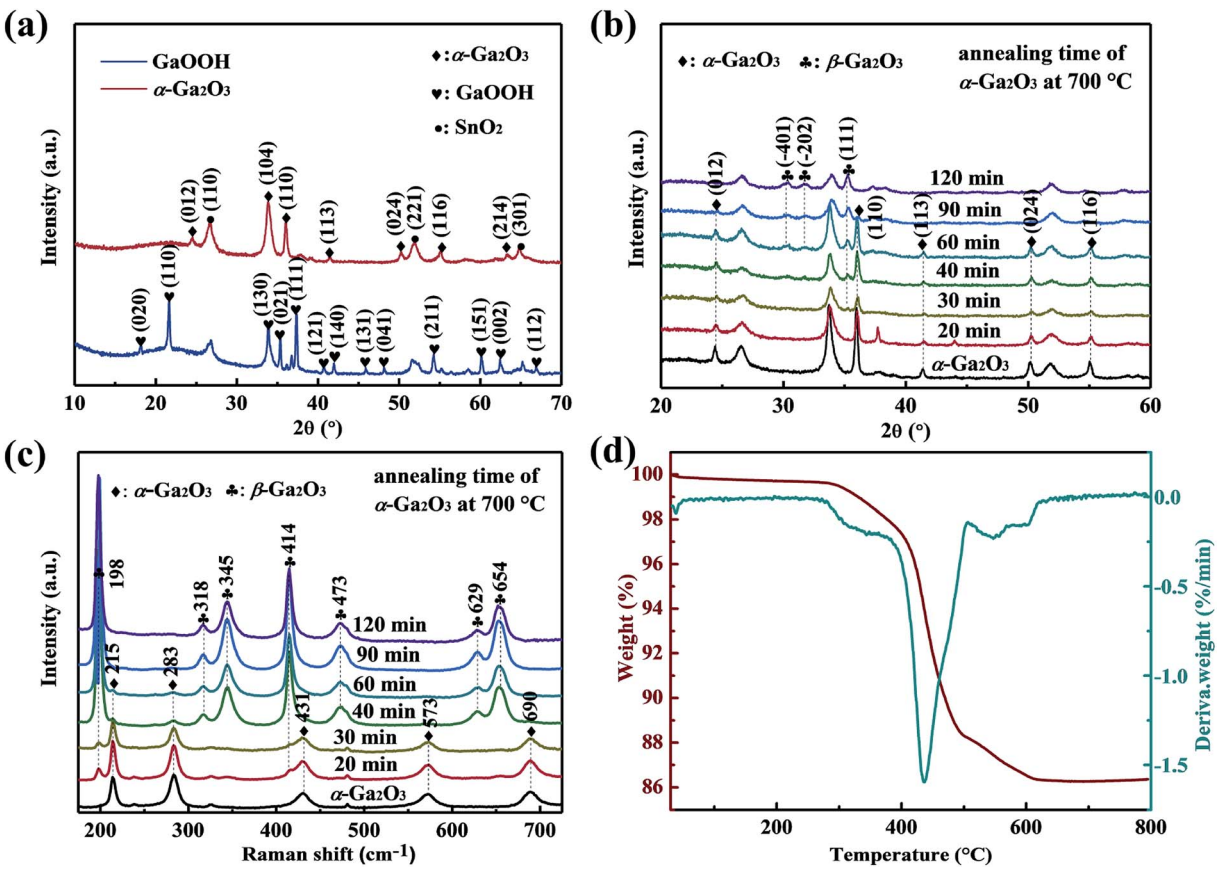

Fig. 2 (a) XRD patterns of as-synthesized GaOOH and α-Ga_2O_3 NRAs. (b) XRD patterns and (c) UV Raman spectra of α-Ga_2O_3 NRAs annealed in air at 700 °C for various times. (d) TG/DTG curve of the as-prepared GaOOH NRAs precursor by heating from room temperature to 800 °C in air.

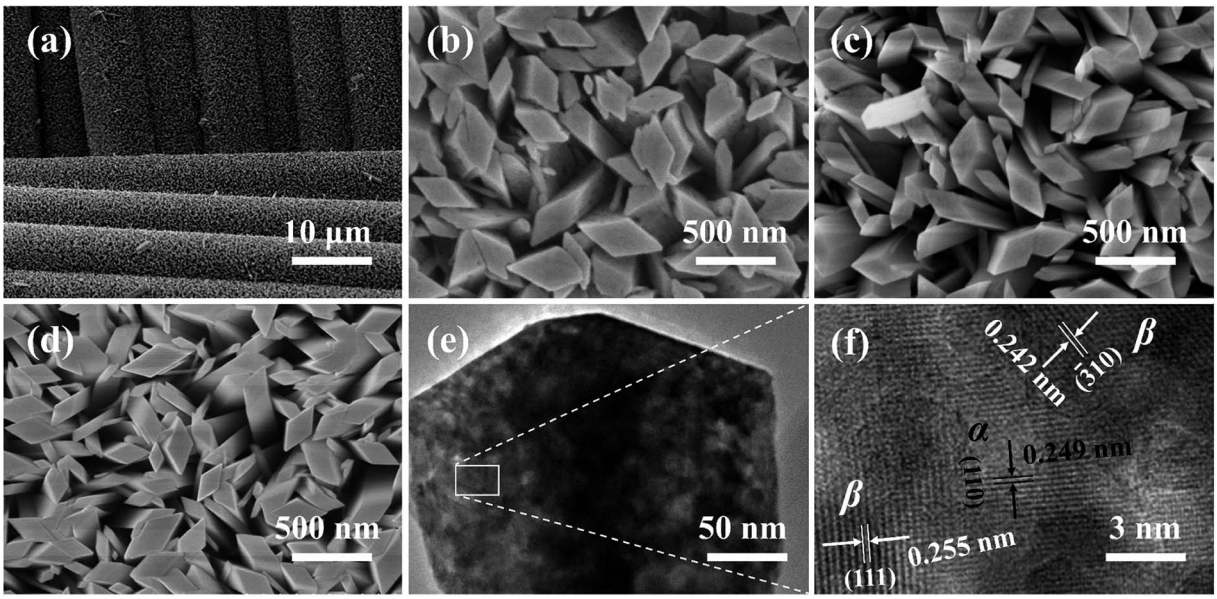

Fig. 3 (a) SEM images of α-Ga_2O_3 NRAs. High-magnification SEM images of (b) α-Ga_2O_3 NRAs, (c) Ga_2O_3-60 NRAs, (d) β-Ga_2O_3 NRAs. (e) Low and high resolution TEM images of (f).

existing Raman bands of α-Ga_2O_3, indicating the formation of β-Ga_2O_3. However, only Raman bands at 215 cm^{-1} and 283 cm^{-1} attributed to α-Ga_2O_3 are detected with annealing time to 60 min, and both disappeared at 90 min. The result is unsynchronized with that revealed by the XRD patterns, which can be attributed to the strong sensitivity of UV Raman spectroscopy to the surface region, and XRD mainly reflects the bulk information of materials.[47] Based on the above results, we suggest that the samples annealed for 20–90 min are α/β-Ga_2O_3 phase junction. In the following sections, the α-Ga_2O_3 NRAs annealed at 700 °C for various time will be labeled as Ga_2O_3-20 (annealed for 20 min), Ga_2O_3-30 (annealed for 30 min), Ga_2O_3-40 (annealed for 40 min), Ga_2O_3-60 (annealed for 60 min), Ga_2O_3-90 (annealed for 90 min) and β-Ga_2O_3 NRAs (annealed for 120 min), respectively.

The TG/DTG curve of the as-prepared GaOOH NRAs precursor by heating from room temperature to 800 °C in air atmosphere is shown in Fig. 2(d). A major weight loss of 11.2% can be noticed in the temperature range of approximately 260–480 °C, with the fastest weight loss rate occurring at 438 °C, which is attributed to transformation of GaOOH into α-Ga_2O_3 by thermal dehydration. A weak weight loss of 2% is also noted at the range of 500–630 °C, indicating the conversion of α-Ga_2O_3 to β-Ga_2O_3. With further prolonged heating up to 800 °C, there is no weight loss.

A typical SEM image of as-synthesized α-Ga_2O_3 NRAs, as presented in Fig. 3(a), which reveals the uniform and dense growth of the sample on each fiber rod. High-magnification SEM images of α-Ga_2O_3 NRAs and other Ga_2O_3 NRAs obtained by annealing (Ga_2O_3-60 and β-Ga_2O_3) are also shown in Fig. 3(b–d), respectively. Further revealing that the diameter of all nanorods ranged from 100 to 400 nm and the tips are all diamond-shaped. The annealing process has not significantly changed the morphology of Ga_2O_3 NRAs.[51] Fig. 3(e and f) shows the low and high resolution TEM images of the Ga_2O_3-60 NRAs. Different lattice fringes are observed in here. The lattice-spacing value of 0.249 nm matches the (110) planes of α-Ga_2O_3, while the lattice-spacing values of 0.242 nm and 0.255 nm are ascribed to the (−310) and (111) planes of β-Ga_2O_3. This result clearly demonstrates the formation of α/β heterophase junctions in Ga_2O_3-60 NRAs, supporting the previous analysis of XRD and UV Raman spectroscopy.

The photocatalytic activities of Ga_2O_3 NRAs were evaluated by the degradation of RhB aqueous solution under UV light irradiation. A typical UV-vis absorption spectrum of RhB aqueous solution during photocatalytic degradation process in the presence of the Ga_2O_3 NRAs is shown in Fig. S1.† The decrease of the characteristic peak at 554 nm during illumination suggests RhB decomposition.[1,43] Fig. 4(a) and S2† reveals the comparison of photocatalytic activities of different Ga_2O_3 NRAs. Among them, the Ga_2O_3-60 NRAs exhibits the best photocatalytic with a degradation rate of 97%, which can be attributed to the α/β-Ga_2O_3 phase junction promoting the separation of photogenerated electrons and holes.[47] Furthermore, the photocatalytic degradation process of these Ga_2O_3 NRAs were fitted using the first-order kinetic curve according to the Langmuir–Hinshelwood model.[32,52] As shown in Fig. 4(b), the value of the reaction rate constant (K) are estimated to be 0.0232, 0.0301, 0.0265, 0.0245, 0.0589, 0.0546 and 0.0418 min^{-1}, corresponding to the α-Ga_2O_3, Ga_2O_3-20, Ga_2O_3-30, Ga_2O_3-40, Ga_2O_3-60, Ga_2O_3-90 and β-Ga_2O_3 NRAs, respectively.

Generally, a series of photogenerated reactive species, such as h^+, $^{\bullet}O_2^-$ and $^{\bullet}OH$, are involved in the photocatalytic process.[4,53] To reveal the main reactive species responsible for the degradation of RhB solution by the Ga_2O_3-60 NRAs, radical trapping experiments were performed by adding EDTA

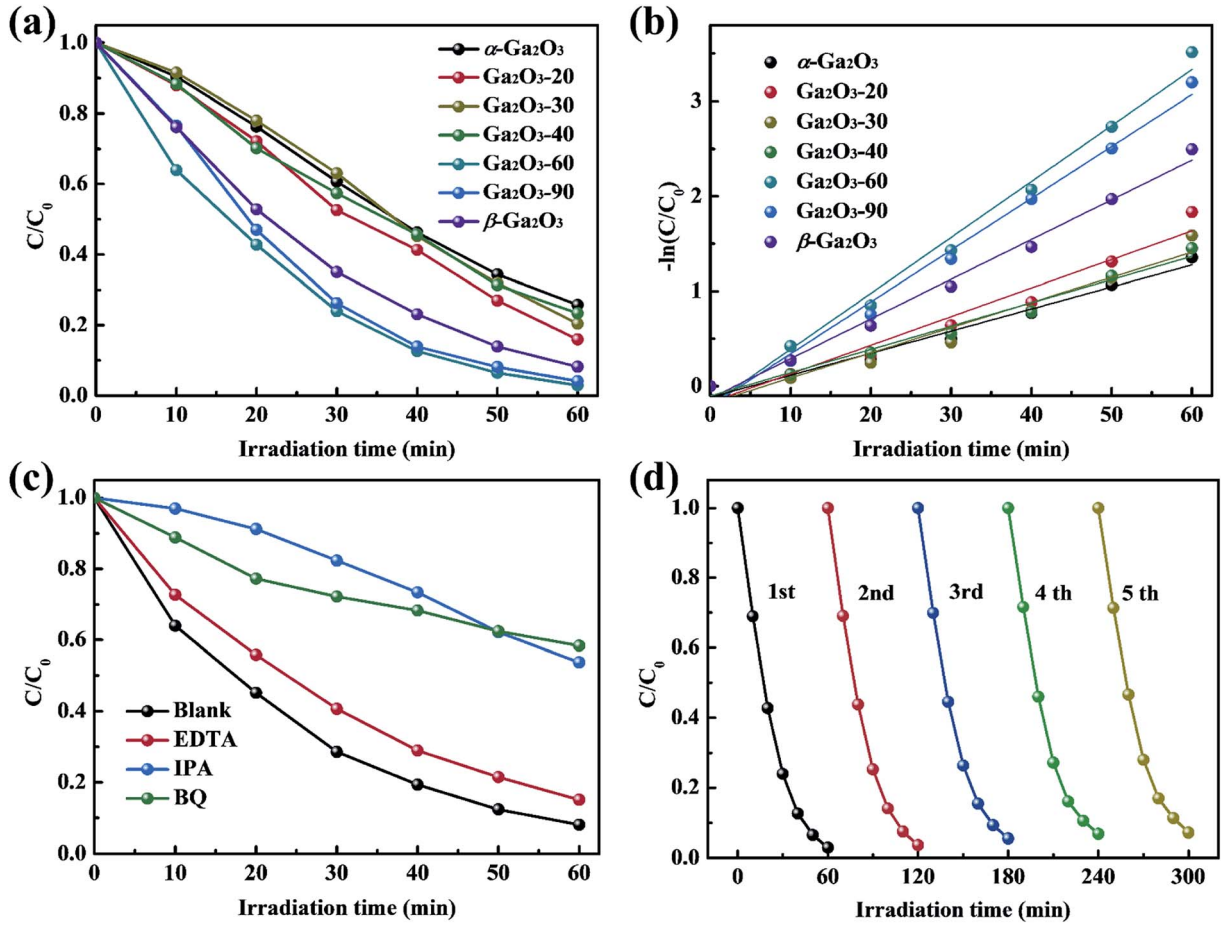

Fig. 4 (a) Photocatalytic degradation of RhB in the presence of different Ga_2O_3 NRAs and (b) corresponding kinetic linear simulation curves. (c) Effect of trapping agents on the photocatalytic degradation of RhB over the Ga_2O_3-60 NRAs. (d) Photocatalytic stability test of the Ga_2O_3-60 NRAs in recycling reactions.

(ethylenediamine tetraacetic acid, h^+ trapping agents), IPA (isopropyl alcohol, $^{\bullet}OH$ trapping agents) and BQ (benzoquinone, $^{\bullet}O_2^-$ trapping agents), respectively. As shown in Fig. 4(c), the photocatalytic activity of the Ga_2O_3-60 NRAs is affected slightly with the addition of EDTA, indicating that h^+ is not the main factor in this system. In contrast, the introduction of IPA or BQ greatly suppressed the photocatalytic activity of the Ga_2O_3-60 NRAs, indicating that $^{\bullet}OH$ and $^{\bullet}O_2^-$ acted as dominating reactive species in the reaction system.

Moreover, the cycling stability of the Ga_2O_3-60 NRAs was evaluated by conducting five consecutive cycle degradation experiments. As shown in Fig. 4(d), the degradation ratio of RhB is not obviously reduced during the repeated experiments, indicating the remarkable stability of the Ga_2O_3-60 NRAs. XRD patterns (Fig. S3†) also indicates that no structural difference can be observed between the Ga_2O_3-60 NRAs before and after photocatalytic degradation of RhB solution.

For the proposed photocatalytic degradation mechanism of the system, the band structures of α-Ga_2O_3 and β-Ga_2O_3 were characterized by Mott–Schottky measurements and XPS. As shown in Fig. 5(a and b), the flat band potential of α-Ga_2O_3 is calculated to be −1.26 eV (*vs.* SCE), which is more negative than the −0.96 eV (*vs.* SCE) of β-Ga_2O_3, and the valence band potential of β-Ga_2O_3 is 3.05 eV, which is more positive than the 2.92 eV of α-Ga_2O_3. Further combined with the band gap of Ga_2O_3 reported in our previous work,[51] a schematic illustration of photocatalytic reaction process and charge separation transfer of α/β-Ga_2O_3 phase junction under UV light irradiation is shown in Fig. 5(c). Under UV light irradiation, the internal electric field of the α/β-Ga_2O_3 phase junction could drive the photogenerated charge transfer, promoting the photogenerated electrons transfer from the α phase to the β phase, and the photogenerated holes transfer from the β phase to the α phase. Following that, the photogenerated electrons react with O_2 to generate $^{\bullet}O_2^-$ and the photogenerated holes oxidize OH^- to $^{\bullet}OH$, which together involve in RhB degradation. Efficient charge separation inhibits their recombination, resulting in improved photocatalytic degradation performance.[47,49] In addition, it should be mentioned that phase junction can form on both the surface of Ga_2O_3 and in the bulk. Although almost no phase junctions were observed on the surface of the Ga_2O_3-60 NRAs, they still function as charge separation centers in the bulk. The separated carriers eventually diffuse to the surface of the sample to participate in the photocatalytic reaction.[4] On the

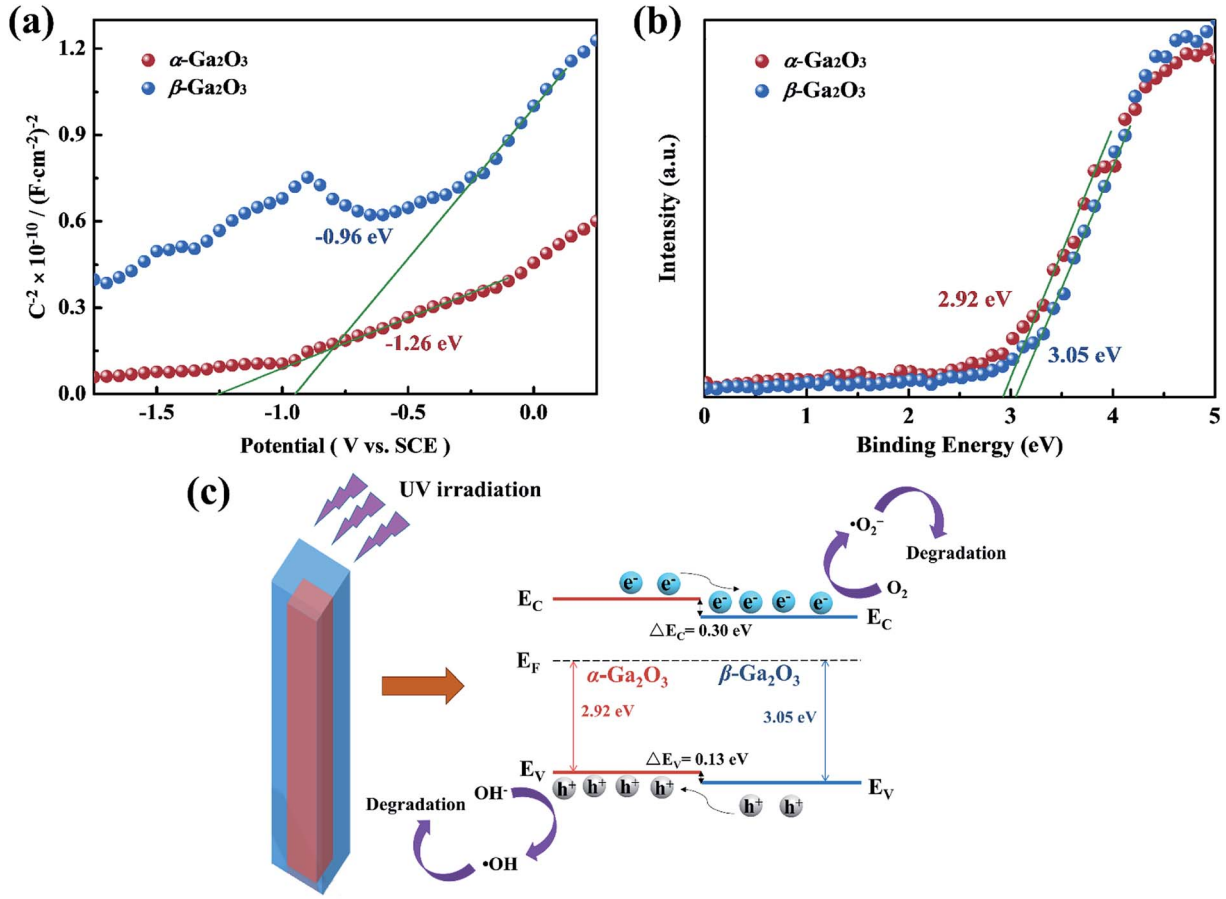

Fig. 5 (a) Mott–Schottky curves of α-Ga_2O_3 NRAs and β-Ga_2O_3 NRAs electrodes measured in 0.5 M Na_2SO_4 solution. (b) XPS valence band spectra of α-Ga_2O_3 NRAs and β-Ga_2O_3 NRAs. (c) Schematic illustration of photocatalytic reaction process and charge separation transfer of α/β-Ga_2O_3 phase junction under UV light irradiation.

other hand, for Ga_2O_3 as a photocatalytic degradation material, the performance of the β phase is generally better than that of the α phase,[7,43] which is confirmed in Fig. 4(a) of this research. Therefore, in addition to the efficient charge separation due to the phase junction in the bulk, the excellent photocatalytic activity of the Ga_2O_3-60 NRAs is also derived from the inherently high activity of the β surface phase. Interestingly, the Ga_2O_3-20, Ga_2O_3-30 and Ga_2O_3-40 NRAs did not exhibit excellent photocatalytic activity despite the formation of phase junctions on various surfaces. The phase transformation of Ga_2O_3 is a surface-preferred process, which is accompanied by the formation of defects.[54] These defects may become the recombination center of photogenerated electron–hole pairs, reducing the number of efficient carriers on the surface.[55] As

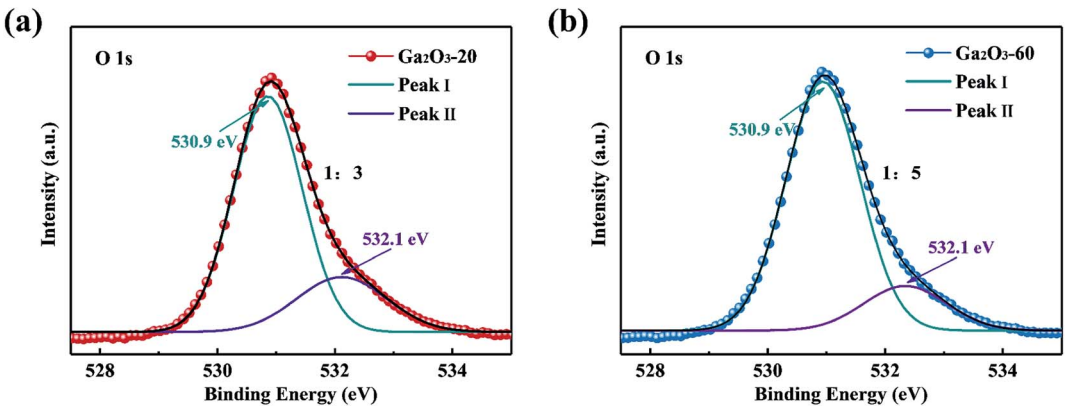

Fig. 6 O 1s XPS spectra of (a) Ga_2O_3-20 NRAs and (b) Ga_2O_3-60 NRAs.

Table 1 Comparison of the photocatalytic activity of a selection of previously reported Ga_2O_3 related materials and this work

Photocatalyst, concentration (mg L^{-1})	Pollutants, concentration (mol L^{-1})	Light source	Degradation after 60 min	Reference
α-Ga_2O_3 nanoplates, 90	RhB, 0.45×10^{-5}	AM 1.5 solar simulator	53%	1
α-Ga_2O_3 nanoparticles, 400	TC, 5.6×10^{-5}	30 W UV lamp	85%	5
α-Ga_2O_3 nanorods, 1000	RhB, 0.84×10^{-5}	300 W Hg lamp	62%	33
β-Ga_2O_3 nanorods, 1000	RhB, 2×10^{-5}	150 W xenon lamp	39%	36
β-Ga_2O_3 microspheres, 1000	RhB, 2×10^{-5}	150 W xenon lamp	60%	37
Ga_2O_3 sheet, 500	CR, 2.15×10^{-5}	30 W UV lamp	33%	38
β-Ga_2O_3 nanorods, 1000	RhB, 2×10^{-4}	1000 W UV lamp	38%	43
TiO_2–Ga_2O_3 heterojunctions	MO, 1.8×10^{-5}	30 W UV lamp	83%	45
α/β-Ga_2O_3 NRAs, 200	RhB, 2×10^{-5}	10 W UV lamp	97%	This work

a result, the photocatalytic activity of the initially annealed Ga_2O_3 phase junction NRAs was not satisfactory.

To obtain more insight into the effect of defects on photocatalytic activity, the Ga_2O_3-20 NRAs and Ga_2O_3-60 NRAs were selected as typical samples for XPS analysis. As shown in Fig. 6, the O 1s spectra could be divided into two peaks: I and II, representing lattice oxygen ions and oxygen ions in the oxygen vacancies region, respectively.[28] The peak ratio (II/I) of the Ga_2O_3-20 NRAs is 1/3, which is higher than that of the Ga_2O_3-60 NRAs (1/5), indicating the presence of more oxygen vacancies. Obviously, the Ga_2O_3-20 NRAs exhibits poor photocatalytic activity due to the existence of abundant oxygen vacancy defects.

The comparison of the photocatalytic degradation activity of α/β-Ga_2O_3 phase junction NRAs in this work and other previously reported Ga_2O_3 related materials is listed in Table 1. Although the comparison of photocatalytic activity is not absolutely reasonable due to the different light source conditions and pollutants used in each experiment, the photocatalytic activity of α/β-Ga_2O_3 phase junction NRAs in this work is significantly superior to almost all previous reports on Ga_2O_3 related materials. This method has realized the large-area growth of α/β-Ga_2O_3 phase junction NRAs on the flexible glass fiber fabric and obviously improved its photocatalytic performance, which is of great significance in the future research in the field of photocatalysis.

4. Conclusions

In summary, large-area Ga_2O_3 NRAs with controllable α/β phase junction were firstly prepared *in situ* on a flexible glass fiber fabric by a facile and environmentally friendly three-step method. Photocatalytic degradation experiments showed that the α/β-Ga_2O_3 phase junction NRAs synthesized by annealing α-Ga_2O_3 NRAs at 700 °C for 60 min exhibited remarkable performance for RhB, with a degradation rate of 97% in 60 min under UV light. The enhanced photocatalytic activity can be attributed to the unique phase junction promoting efficient charge separation and inhibiting the recombination of photogenerated electron–hole pairs. Additionally, the glass fiber fabric can realize large-area growth of the Ga_2O_3 NRAs, effectively solve the trouble of difficult recovery and reuse of photocatalysts, as well as the insufficient absorption of light. A facile environmentally friendly and inexpensive synthesis route will open new avenues for the development of efficient photocatalysts.

Conflicts of interest

There are no conflicts to declare.

Acknowledgements

This work was supported by the National Natural Science Foundation of China (No. 61704153, 51572241, 61774019, 51572033), Natural Science Foundation of Zhejiang Province (No. LY20F040005), Zhejiang Public Service Technology Research Program/Analytical Test (LGC19F040001), and Fundamental Research Funds of Zhejiang Sci-Tech University (2019Q061, 2019Q067).

References

1 N. Syed, A. Zavabeti, M. Mohiuddin, B. Zhang, Y. Wang, R. S. Datta, P. Atkin, B. J. Carey, C. Tan, J. van Embden, A. S. R. Chesman, J. Z. Ou, T. Daeneke and K. Kalantar-zadeh, *Adv. Funct. Mater.*, 2017, **27**, 1702295.
2 J. Wei, F. Guo, X. Wang, K. Xu, M. Lei, Y. Liang, Y. Zhao and D. Xu, *Adv. Mater.*, 2018, **30**, 1805153.
3 W. Zhong, S. Shen, S. Feng, Z. Lin, Z. Wang and B. Fang, *CrystEngComm*, 2018, **20**, 7851–7856.
4 Y. Wang, W. Zhang, Z. Wang, Y. Cao, J. Feng, Z. Wang and Y. Ma, *Chin. J. Catal.*, 2018, **39**, 1500–1510.
5 J. Liu, W. Lu, Q. Zhong, H. Wu, Y. Li, L. Li and Z. Wang, *J. Colloid Interface Sci.*, 2018, **519**, 255–262.
6 X. He, S. Z. Luan, L. Wang, R. Y. Wang, P. Du, Y. Y. Xu, H. J. Yang, Y. G. Wang, K. Huang and M. Lei, *Mater. Lett.*, 2019, **244**, 78–82.
7 J. Liu and G. Zhang, *Mater. Res. Bull.*, 2015, **68**, 254–259.
8 L. C. Tien, W. T. Chen and C. H. Ho, *J. Am. Ceram. Soc.*, 2011, **94**, 3117–3122.
9 Z. Dong, J. Pan, B. Wang, Z. Jiang, C. Zhao, J. Wang, C. Song, Y. Zheng, C. Cui and C. Li, *J. Alloys Compd.*, 2018, **747**, 788–795.
10 W. Zhong, Y. Lou, S. Jin, W. Wang and L. Guo, *Sci. Rep.*, 2016, **6**, 23235.

11 K. Huang, J. Liu, L. Wang, G. Chang, R. Wang, M. Lei, Y. Wang and Y. He, *Appl. Surf. Sci.*, 2019, **487**, 1145–1151.
12 W. Zhong, J. Huang, S. Liang, J. Liu, Y. Li, G. Cai, Y. Jiang and J. Liu, *ACS Energy Lett.*, 2019, **5**, 31–38.
13 S. Lin, X. Bai, H. Wang, H. Wang, J. Song, K. Huang, C. Wang, N. Wang, B. Li and M. Lei, *Adv. Mater.*, 2017, **29**, 1703238.
14 A. A. Ismail, I. Abdelfattah, M. Faisal and A. Helal, *J. Hazard. Mater.*, 2018, **342**, 519–526.
15 W. Zhong, S. Shen, M. He, D. Wang, Z. Wang, Z. Lin, W. Tu and J. Yu, *Appl. Catal., B*, 2019, **258**, 117967.
16 Y. Ma, X. Zhao, M. Niu, W. Li, X. Wang, C. Zhai, T. Wang, Y. Tang and X. Dai, *RSC Adv.*, 2017, **7**, 4124–4134.
17 A. Kakoria, B. Devi, A. Anand, A. Halder, R. R. Koner and S. Sinha-Ray, *ACS Appl. Nano Mater.*, 2018, **2**, 64–74.
18 S. Wang, H. Sun, Z. Wang, X. Zeng, G. Ungar, D. Guo, J. Shen, P. Li, A. Liu, C. Li and W. Tang, *J. Alloys Compd.*, 2019, **787**, 133–139.
19 J. Yu, Z. Nie, L. Dong, L. Yuan, D. Li, Y. Huang, L. Zhang, Y. Zhang and R. Jia, *J. Alloys Compd.*, 2019, **798**, 458–466.
20 J. Zhang, S. Jiao, Y. Wan, S. Gao, D. Wang and J. Wang, *CrystEngComm*, 2018, **20**, 4329–4335.
21 H. Lu, S. Jiao, Y. Nie, S. Liu, S. Gao, D. Wang, J. Wang, L. Li and X. Wang, *J. Alloys Compd.*, 2020, **823**, 153903.
22 C. Wu, D. Guo, L. Zhang, P. Li, F. Zhang, C. Tan, S. Wang, A. Liu, F. Wu and W. Tang, *Appl. Phys. Lett.*, 2020, **116**, 072102.
23 M. Baldini, Z. Galazka and G. Wagner, *Mater. Sci. Semicond. Process.*, 2018, **78**, 132–146.
24 X. Wang, Y. Cui, T. Li, M. Lei, J. Li and Z. Wei, *Adv. Opt. Mater.*, 2018, **7**, 1801274.
25 H. Zhang, L. Yuan, R. Jia, X. Tang, J. Hu, Y. Zhang, Y. Zhang and J. Sun, *J. Phys. D: Appl. Phys.*, 2019, **52**, 215104.
26 D. Guo, Y. Su, H. Shi, P. Li, N. Zhao, J. Ye, S. Wang, A. Liu, Z. Chen, C. Li and W. Tang, *ACS Nano*, 2018, **12**, 12827–12835.
27 L. Dong, J. Yu, R. Jia, J. Hu, Y. Zhang and J. Sun, *Opt. Mater. Express*, 2019, **9**, 1191.
28 D. Guo, H. Liu, P. Li, Z. Wu, S. Wang, C. Cui, C. Li and W. Tang, *ACS Appl. Mater. Interfaces*, 2017, **9**, 1619–1628.
29 J. Zhang, S. Jiao, D. Wang, S. Ni, S. Gao and J. Wang, *J. Mater. Chem. C*, 2019, **7**, 6867–6871.
30 H. J. Lin, H. Gao and P. X. Gao, *Appl. Phys. Lett.*, 2017, **110**, 043101.
31 A. Pérez-Tomás, E. Chikoidze, Y. Dumont, M. R. Jennings, S. O. Russell, P. Vales-Castro, G. Catalan, M. Lira-Cantú, C. Ton-That, F. H. Teherani, V. E. Sandana, P. Bove and D. J. Rogers, *Mater. Today Energy*, 2019, **14**, 100350.
32 S. Jin, W. Lu, P. C. Stanish and P. V. Radovanovic, *Chem. Phys. Lett.*, 2018, **706**, 509–514.
33 D. Li, X. Duan, Q. Qin, H. Fan and W. Zheng, *J. Mater. Chem. A*, 2013, **1**, 12417.
34 X. Zhang, H. Huang, Y. Zhang, D. Liu, N. Tong, J. Lin, L. Chen, Z. Zhang and X. Wang, *ACS Omega*, 2018, **3**, 14469–14476.
35 H. Liu, Z. Wang, H. Li, X. Zhang, X. Qin, Y. Dai, P. Wang, Y. Liu and B. Huang, *RSC Adv.*, 2018, **8**, 14328–14334.
36 K. Girija, S. Thirumalairajan, A. K. Patra, D. Mangalaraj, N. Ponpandian and C. Viswanathan, *Semicond. Sci. Technol.*, 2013, **28**, 035015.
37 K. Girija, S. Thirumalairajan, V. R. Mastelaro and D. Mangalaraj, *J. Mater. Chem. A*, 2015, **3**, 2617–2627.
38 M. Bagheri and A. R. Mahjoub, *RSC Adv.*, 2016, **6**, 87555–87563.
39 C. Han, W. Mao, K. Bao, H. Xie, Z. Jia and L. Ye, *Int. J. Hydrogen Energy*, 2017, **42**, 19913–19919.
40 S. Hong, C. K. Rhee and Y. Sohn, *J. Alloys Compd.*, 2019, **774**, 11–17.
41 W. Zhang, B. S. Naidu, J. Z. Ou, A. P. O'Mullane, A. F. Chrimes, B. J. Carey, Y. Wang, S. Y. Tang, V. Sivan, A. Mitchell, S. K. Bhargava and K. Kalantar-Zadeh, *ACS Appl. Mater. Interfaces*, 2015, **7**, 1943–1948.
42 S. Kikkawa, K. Teramura, H. Asakura, S. Hosokawa and T. Tanaka, *J. Phys. Chem. C*, 2018, **122**, 21132–21139.
43 L. S. Reddy, Y. H. Ko and J. S. Yu, *Nanoscale Res. Lett.*, 2015, **10**, 364.
44 S. Luan, L. Dong, X. Ma and R. Jia, *J. Alloys Compd.*, 2020, **812**, 152026.
45 H. Xu, F. Han, C. Xia, S. Wang, R. K. Ramachandran, C. Detavernier, M. Wei, L. Lin and S. Zhuiykov, *Nanoscale Res. Lett.*, 2019, **14**, 163.
46 X. Wang and C. Li, *J. Phys. Chem. C*, 2018, **122**, 21083–21096.
47 X. Wang, Q. Xu, M. Li, S. Shen, X. Wang, Y. Wang, Z. Feng, J. Shi, H. Han and C. Li, *Angew. Chem., Int. Ed.*, 2012, **51**, 13089–13092.
48 D. Guo, K. Chen, S. Wang, F. Wu, A. Liu, C. Li, P. Li, C. Tan and W. Tang, *Phys. Rev. Appl.* , 2020, **13**, 24051.
49 Y. Wang, Q. Wang, X. Zhan, F. Wang, M. Safdar and J. He, *Nanoscale*, 2013, **5**, 8326–8339.
50 C. He, D. Guo, K. Chen, S. Wang, J. Shen, N. Zhao, A. Liu, Y. Zheng, P. Li, Z. Wu, C. Li, F. Wu and W. Tang, *ACS Appl. Nano Mater.*, 2019, **2**, 4095–4103.
51 K. Chen, S. Wang, C. He, H. Zhu, H. Zhao, D. Guo, Z. Chen, J. Shen, P. Li, A. Liu, C. Li, F. Wu and W. Tang, *ACS Appl. Nano Mater.*, 2019, **2**, 6169–6177.
52 B. Das, B. Das, N. S. Das, S. Sarkar and K. K. Chattopadhyay, *Microporous Mesoporous Mater.*, 2019, **288**, 109600.
53 S. Wang, D. Li, C. Sun, S. Yang, Y. Guan and H. He, *Appl. Catal., B*, 2014, **144**, 885–892.
54 V. Ghodsi, S. Jin, J. C. Byers, Y. Pan and P. V. Radovanovic, *J. Phys. Chem. C*, 2017, **121**, 9433–9441.
55 D. Y. Guo, Z. P. Wu, Y. H. An, X. C. Guo, X. L. Chu, C. L. Sun, L. H. Li, P. G. Li and W. H. Tang, *Appl. Phys. Lett.*, 2014, **105**, 023507.

